TEST
https://doi.org/10.1007/s11749-021-00768-w

ORIGINAL PAPER

Two-way layout factorial experiments of spatial point pattern responses in mineral flotation

Jonatan A. González[1] · **Bernardo M. Lagos-Álvarez**[2] · **Jorge Mateu**[1]

Received: 9 December 2019 / Accepted: 10 March 2021

Abstract
Factorial experiments are well-understood when the given observations are outcomes of random variables. However, when we observe spatial point patterns in each combination of factors cells, the methodology is much less developed. Motivated by a real problem of locations of bubbles in a mineral flotation experiment where the interest is analysing if the spatial distribution might be affected by frother concentrations and volumetric airflow rates, we develop an approach for statistical testing of two-way factorial experiments for spatial point patterns. We describe the point patterns through the K-function, a second-order summary statistic, and develop a set of new Fisher-based statistics using weighted means. For inference by Monte Carlo, we use random permutations of weighted residuals depending on the null hypothesis. We conduct simulation experiments to demonstrate the performance of the new test statistics and present the results of the real problem.

Keywords Flotation bubble data · Frother concentration · K-function · Permutation test · Replicated point patterns · Volumetric airflow rate

Mathematics Subject Classification 60G55 · 62M30

1 Introduction and data

The copper production process consists of a large number of steps that allow obtaining cathodes from a mineral deposit. The ore, once it has been extracted from a mine, passes through successive stages of a comminution process. In the case of copper oxide ores, the subsequent processing steps correspond to hydrometallurgy and electrometallurgy. For sulphide ores, after the comminution, the processing requires steps of concentration by flotation and pyrometallurgy (Schlesinger et al. 2011, Chap. 3).

✉ Jonatan A. González
jmonsalv@uji.es

[1] Department of Mathematics, University Jaume I, Castellón, Spain

[2] Department of Statistics, University of Concepción, Concepción, Chile

Published online: 25 March 2021

Mineral flotation process allows separating particles from non-metallic gangue particles. The comminuted material is deposited in reactors (flotation cells) forming a pulp with water and some reagents. The mineral particles, being recovered after the flotation cell is aerated and agitated, attach to the bubbles and rise to the surface where they form a blanket of froth containing the mineral.

In order to quantify the hydrodynamic performance within flotation cells, a series of so-called *gas dispersion characteristics* are defined. One of the most important is the *bubble size distribution* BSD, characterised by a random bubble diameter. The bubble size distribution is a very complicated variable to be measured (Kracht et al. 2013). One of the sampling techniques for measuring it is the *sampling-followed-by-imaging* (Gomez and Finch 2007; Miskovic and Luttrell 2012). Some further approaches have been applied in the literature to analyse BSD by using methods from stochastic geometry such as Boolean models (Emery et al. 2012; Kracht et al. 2013). These approaches lead to calculate, for instance, the diameters and the BSD directly from the binary image by taking advantage of the assumption of *complete spatial randomness*, which is usually taken for granted.

The spatial distribution of the bubbles has not been addressed in the literature. Understanding this distribution or even properly modelling it can be essential for the proper operation of flotation machines, and the recovery of metal particles. This distribution may depend on the variables that are controlled in the experiment. It is known that the flotation characteristics are strongly dependent on a variety of important operating and design factors (Gómez et al. 2016).

The volumetric airflow rate (L min^{-1}) and the specific frother concentration (ppm) are two factors that particularly influence the physical properties (Laskowski 2001; Gómez et al. 2016). Therefore, we are interested in these two factors as they could be potentially influential in the spatial distribution of the bubbles.

High-resolution images (170 pixels/mm) were recorded by using a Nikon D-5100 photo camera with a macrolens of 60 mm; the camera was adjusted manually always to achieve the same dimensions in all the photographs of the experiment. Thus, the images have dimensions 29.0 mm $\times$ 19.2 mm. Figure 1 displays two images of bubbles generated in a flotation machine.

When the bubble images have been successfully recorded following the procedure described above, they are processed through classical image analysis. They are con-

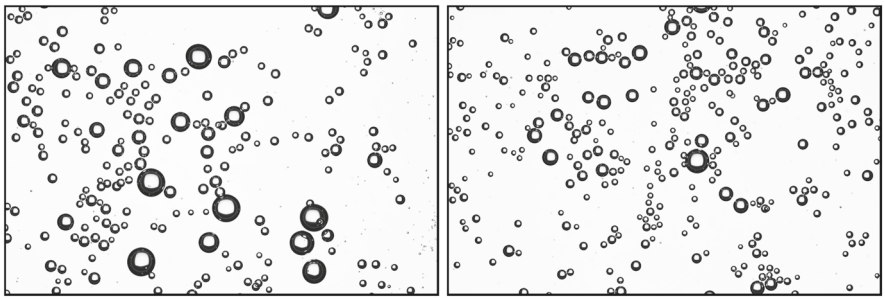

Fig. 1 Two images of bubbles in a flotation machine

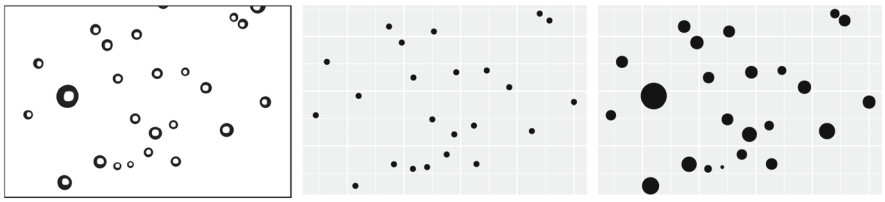

Fig. 2 An image of bubbles in a flotation cell (left) and its corresponding point patterns where points are centres of bubbles (centre) and the bubbles size is attached to centres locations as marks (right)

verted into binary images and processed to identify bubbles (segmentation); then, the bubbles in the image are classified in categories by their position and metrics (classification) (Kracht et al. 2013). The analysis of such images is developed to record some characteristics such as the bubbles themselves, the locations of their centroids, diameters, and areas. Our dataset consists of 54 images containing a total of 8385 floating bubbles. The images of bubbles can be regarded as spatial point patterns where the centroids correspond to the points, and where other characteristics can be attached as quantitative marks. An example of a typical bubble point pattern is shown in Fig. 2.

We have in the dataset three frother concentration levels, 5 ppm, 10 ppm and 15 ppm, as well as three volumetric airflow rate levels, $5\,\mathrm{L\,min^{-1}}$, $8\,\mathrm{L\,min^{-1}}$ and $10\,\mathrm{L\,min^{-1}}$. Additionally, we have six replicates (point patterns) at each combination of levels of such factors. The treatment combinations of the experiment, as well as the observed bubble point patterns, are represented in Fig. 3.

In classical statistics, factorial experiments allow evaluating the combined effects of two or more experimental variables. The information obtained in this type of experiments is much more complete than that obtained through a series of single-factor experiments since factorial experiments allow the study of the interaction of the factors. The problem we are facing here is considering factorial experiments when the observations are spatial point patterns rather than numeric random variables.

The analysis of this type of experiments when the observations are not quantitative variables is in its infancy, especially in the field of point processes. A few authors have treated the observations in an experiment when they are point patterns (Diggle et al. 1991; Baddeley et al. 1993; Diggle et al. 2000; Hahn 2012; Hahn and Vedel Jensen 2016), and their studies have concentrated mainly on the comparison of several groups of responses (a single factor). Some other authors have included, for example, non-spatial variables or mixed effects in their models (Landau and Everall 2008; Myllymäki et al. 2014; Bagchi and Illian 2015). Finally, only a few works have been focused on factorial experiments; for instance, Ramón et al. (2016) extended Diggle et al.'s method (Diggle et al. 1991) to the two factors case through a quite pragmatic approach.

On the other hand, methods for the analysis of variance when observations are functions are more comprehensive. Fisher-based tests (Cuevas et al. 2004; Ramsay and Silverman 2005; Zhang 2013), L_2-norm based tests (Zhang 2013), basis functions based tests (Górecki and Smaga 2015), wavelets smoothing (Abramovich and Angelini 2006), dimension reduction (Ferraty et al. 2007), and global envelope tests (Mrkvička et al. 2020b), among others, are good examples of the extensive research on ANOVA for functional data.

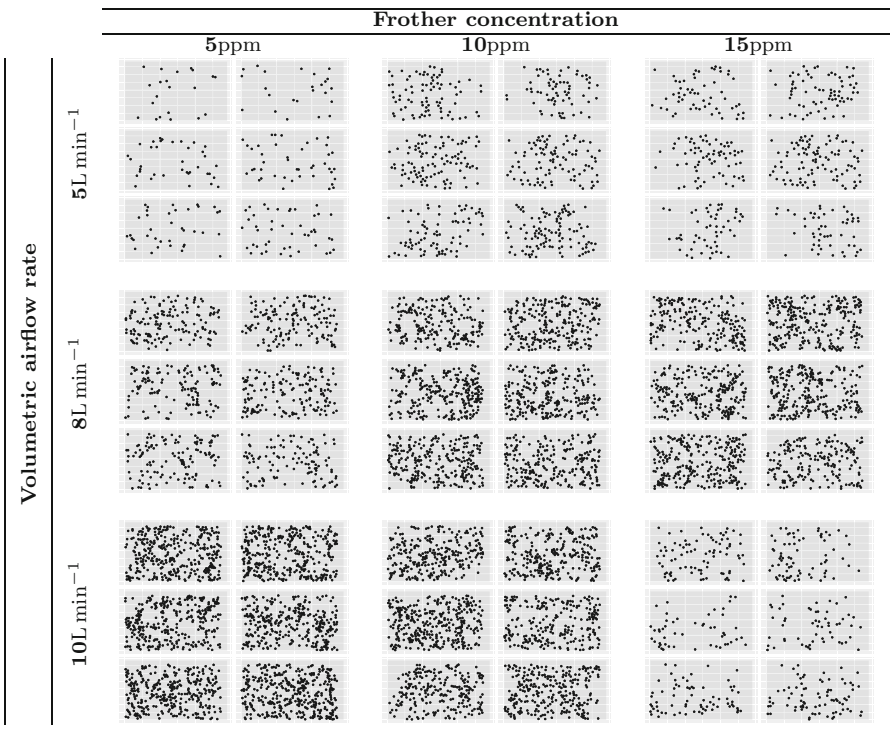

Fig. 3 Arrangement of floating bubbles data. Rows represent the three volumetric airflow rate levels (treatments) and columns the three frother concentration levels. Each cell contains six spatial point patterns (responses)

In this paper, we look at the motivating bubble problem as a case of replicated spatial point patterns, and the goal is to analyse whether the factors or their interactions affect the second-order structure of the point patterns. To fulfil this aim, we develop and provide a new methodology for the analysis of variance in two-way balanced experiments when responses are point patterns. We employ Fisher-based statistics for the tests using weighted means and adopt a permutation strategy of weighted residuals to perform Monte Carlo inference. We note that our statistics are based on the K-function, a second-order summary statistic for spatial point patterns. This function depends on distance and could be treated as a functional measure. However, we are not following this strategy and integrate out such functional dependence on distances.

Section 2 presents some necessary background on point processes. Section 3 develops the methodology for factorial experiments for spatial point patterns. In particular, we use Fisher's test statistics as well as a carefully selected scheme of residuals useful for inference. The bubbles dataset is analysed in Sect. 4. The paper ends with a discussion.

2 Background and set-up

Throughout this paper, we assume that every subset A of $\mathbb{R}^2$ is measurable and any function f defined on $\mathbb{R}$ is integrable in a finite interval $T \subset \mathbb{R}$. We use the notation $\|\cdot\|$ indistinctly to denote the Euclidean vector norm and the L^2-norm. A planar point process is a random, finite or countable collection of points $\mathbf{X} \subset \mathbb{R}^2$ with no accumulation points. A realisation X of a point process can be considered as a finite subset $\{\mathbf{u}_i\}_{i=1}^n \subset W \subset \mathbb{R}^2$. Let $N(A)$ be the number of points of X in $A \subseteq W$. The theory and applications of spatial point processes are discussed extensively in, e.g. Daley and Vere-Jones 2003 and Diggle (2013).

2.1 Ripley's *K*-function

One of the most popular second-order descriptor for analysing point patterns is Ripley's K-function (Ripley 1977). We can use Ripley's K-function in its homogeneous version as long as we assume that the point process is stationary. This function is given by

$$\mathcal{K}(r) = \frac{1}{\lambda}\mathbb{E}\left[\sum_{\mathbf{u}_i \in X} \mathbf{1}\{\|\mathbf{u} - \mathbf{u}_i\| \leq r\} \middle| \mathbf{u} \in \mathbf{X}\right], \tag{1}$$

provided that this value does not depend on the choice of the location $\mathbf{u}$ (see e.g. Møller and Waagepetersen 2004; Baddeley et al. 2015) and where $\|\cdot\|$ represents the Euclidean distance and λ is the first-order intensity of $\mathbf{X}$, i.e. the expected number of points per unit area. In this context, we set $a/0 = 0$ and r belongs to a suitably chosen range $T = (0, r_0]$ (Ho and Chiu 2006). For homogeneous Poisson processes (Diggle 2013), the K-function is $K(r) = \pi r^2$. Note that homogeneous Poisson processes are the archetype of complete spatial random processes (hereinafter CSR). A natural estimator for the K-function is given by

$$\hat{K}(r) = \frac{1}{\hat{\lambda}^2 |W|} \sum_{i=1}^{n} \sum_{j \neq i} \mathbf{1}\{\|\mathbf{u}_i - \mathbf{u}_j\| \leq r\} e(\mathbf{u}_i, \mathbf{u}_j; r), \tag{2}$$

where $|\cdot|$ is, in this case, the area of the set, $e(\mathbf{u}, \mathbf{v}; r)$ is an edge-correction weight (see e.g. Ripley 1988; Baddeley et al. 2015), and $\hat{\lambda}^2$ is an estimator of the squared first-order intensity function, usually given by

$$\hat{\lambda}^2 = \frac{n(n-1)}{|W|^2} \tag{3}$$

where n is the number of points of the pattern X.

We note that we restrict to stationary point patterns motivated by the bubbles experiment producing such point patterns. Recall these come from images all taken under the same conditions, and the distribution of bubbles per concentrations and airflow are homogeneous. Indeed, a favourable argument would be that the stationary K-function

enables underlying inter-point dependence as part of the features of the point pattern model without having to choose one formally. However, our approach can be extended to non-stationary K-functions (Baddeley et al. 2000).

2.2 Pooled estimators

If a summary-statistic function given by a ratio of the form $Y(r) = U(r)/V(r)$ is calculated for a set of n independent observations, then, according to Baddeley et al. (1987); Baddeley et al. (1993, 2015) (and references therein), the *pooled* summary-statistic across replicates, which is unbiased for $Y(r)$ and has minimum variance, is the weighted average of the individual ratios with weights proportional to $V_i(r)$, i.e.

$$\bar{Y}(r) = \frac{\mathbb{E}[U(r)]}{\mathbb{E}[V(r)]} = \frac{\sum_i \hat{U}_i(r)}{\sum_i \hat{V}_i(r)} = \frac{\sum_i \hat{V}_i(r)\hat{Y}_i(r)}{\sum_i \hat{V}_i(r)}.$$

If our summary-statistic is Ripley's K-function, the estimator given in Eq. (2) using the isotropic or the translation edge-correction factors, can be seen as the ratio of two estimators; the numerator is a sum over all pairs of data points, and the denominator corresponds to the number of pairs of distinct points, i.e. $n_i(n_i - 1)$ where n_i is the number of points in the ith point pattern (see e.g. Baddeley et al. 2015). Thus the pooled K-function estimator for a sample $\{\hat{K}_i\}_{i=1}^m$ coming from m point patterns $\{X_i\}_{i=1}^m$, is given by

$$\bar{K}(r) = \frac{1}{\omega_\cdot} \sum_{i=1}^{m} \omega_i \hat{K}_i(r), \quad r \in T, \tag{4}$$

where

$$\omega_i = n_i(n_i - 1), \tag{5}$$

and $\omega_\cdot = \sum_{i=1}^m n_i(n_i - 1)$.

3 Factorial analysis of variance for point patterns

In this section, we adapt the methodology of ANOVA for raw functional data provided by Zhang (2013) to the particular case of functional descriptors associated with spatial point patterns.

3.1 One-way ANOVA

In the literature of point processes, some procedures have been developed to compare the expected values of second-order summary statistics of two or more samples or groups (see e.g. Diggle et al. 1991; Baddeley et al. 1993; Diggle et al. 2000; Hahn

2012). To observe naturally these comparisons, we should consider that the point patterns are grouped by a categorical variable defined as a *factor* in classical linear models, whose different values are called *factor levels*. In this section, we consider weighted means in the statistics for the analysis of variance in the one-way case and establish a unified notation.

We assume that we have m independent samples (groups) $\{\hat{K}_{ij}\}$, $j = 1, \ldots, m_i$, $i = 1, \ldots, m$, with $\{\mathcal{K}_i\}_{i=1}^{m}$ the unknown group means. The main idea is to check the null hypothesis

$$\mathscr{H}_0 : \mathcal{K}_1(r) = \mathcal{K}_2(r) = \cdots = \mathcal{K}_m(r), \quad r \in T,$$

against the alternative

$$\mathscr{H}_1 : \mathcal{K}_i(r) \neq \mathcal{K}_j(r), \text{ for some } i, j \text{ and } r \in T.$$

The group weighted mean function of the m groups is given by

$$\bar{K}_{i\cdot}(r) = \frac{1}{\omega_{i\cdot}} \sum_{j=1}^{m_i} \omega_{ij} \hat{K}_{ij}(r), \quad i = 1, \ldots, m, \tag{6}$$

where the weights ω_{ij} are defined as in Eq. (5). Note that we make the convenient assumption that the groups have the same covariance function, and estimate it jointly. However, for practical purposes and due to the delicate structure of the variance function of Ripley's K-function (Ripley 1988), we directly estimate covariances separately based only on each group (sample). Note also that under the independence of the patterns, the means of the groups remain independent. We define the *pointwise between-treatment variation* as

$$\mathrm{SSH}_m(r) = \sum_{i=1}^{m} m_i \left[\bar{K}_{i\cdot}(r) - \bar{K}_{\cdot\cdot}(r)\right]^2, \tag{7}$$

where $\bar{K}_{\cdot\cdot}(r)$ denotes the overall mean function of the m groups, i.e.

$$\bar{K}_{\cdot\cdot}(r) = \frac{1}{\omega_{\cdot\cdot}} \sum_{i=1}^{m} \omega_{i\cdot} \bar{K}_{i\cdot}(r), \tag{8}$$

where

$$\omega_{\cdot\cdot} = \sum_{i=1}^{m} \sum_{j=1}^{m_i} n_{ij}(n_{ij} - 1). \tag{9}$$

In this case, we can define a L^2-norm-based test through the test statistic given by

$$D_m = \int_T \frac{\mathrm{SSH}_m(r)}{r^2}\mathrm{d}r = \sum_{i=1}^{m} m_i \int_T \frac{1}{r^2}\left[\bar{K}_{i\cdot}(r) - \bar{K}_{\cdot\cdot}(r)\right]^2 \mathrm{d}r.$$

Note that the statistic D_m is Diggle's statistic (Diggle et al. 1991, 2000). Similarly, we can define a statistic that takes into account the variability of particular groups in the sample. Such statistic is the *pointwise within-treatment variation*, and it is given by (see Zhang 2013, p. 329)

$$\mathrm{SSE}_m(r) = \sum_{i=1}^{m} (1 - m_i/m)\,\hat{\sigma}_i(r).$$

where

$$\hat{\sigma}_i(r) = \sum_{j=1}^{m_i}\left[\hat{K}_{ij}(r) - \bar{K}_{i\cdot}(r)\right]^2.$$

We could include the last term into a Fisher-test-type statistic in order to include the sampling variations of the variance functions $\hat{\sigma}_i(r)$, $i = 1, \ldots, m$. In this case, Fisher's statistic is

$$F_m = \frac{\int_T \mathrm{SSH}_m(r)\mathrm{d}r}{\int_T \mathrm{SSE}_m(r)\mathrm{d}r}. \tag{10}$$

3.2 Balanced two-way ANOVA

We have presented in the previous section a model for the analysis of variance with one factor whose levels are used to establish the differences between spatial descriptors (in our case the K-function). In this section, the model is extended to include two factors with fixed levels.

This inclusion is far from trivial as the problem of comparing groups of functional means induced by two factors cannot be solved by simply extending the model of one factor. It is possible that both factors are fixed, both random, or one fixed and one random, and it could be the case that both factors act independently or that the combined action of two factors enhances or inhibits the action of each other in the response function. In the latter case, we say that there is interaction, and we might consider an interaction model. Note that this interaction is not the interaction between points within a point process. When every category of one factor co-occurs in the design with every category of the other factor, we talk about a fully crossed design or a full factorial design (or models). The first approach to this model was proposed, using Ripley's K-function, by Wilson (1998), and Ramón et al. (2016) later applied it. Throughout this work, we focus on a factorial model involving only two fixed factors.

We follow the presentation in Zhang (2013) for the coming ANOVA set-up. Suppose that factor A has a levels and factor B has b levels. Each realisation or replicate contains all ab factorial combinations. In general, there are m_{ij} replicates in each level combination. In this paper, we assume the same number of observations in the cells, i.e. $m_{ij} \equiv c$ for all $i = 1, \ldots, a$ and $j = 1, \ldots, b$,. We have a functional descriptor sample

$$\{\hat{K}_{ijk}\}, i = 1, \ldots, a, j = 1, \ldots, b, k = 1, \ldots, c,$$

where the functional observations can be described by the model

$$\hat{K}_{ijk}(r) = \mathcal{K}_{ij}(r) + \mathscr{E}_{ijk}(r), r \in T, \tag{11}$$

with $\mathscr{E}_{ijk}(r)$ a random error with mean zero. Note that this linear model guarantees the positive sign of the response K-functions. Note the variance functions are supposed to be different across the level combinations, and the functional samples are assumed to be independent. Therefore, model (11) is a heteroscedastic two-way ANOVA model.

For a two-way ANOVA, the mean $\mathcal{K}_{ij}(r)$ can be expressed in the form

$$\begin{aligned} \mathcal{K}_{ij}(r) &= \mathcal{K}_0(r) + \tau_i(r) + \beta_j(r) + (\tau\beta)_{ij}(r), \\ & i = 1, \ldots, a, j = 1 \ldots, b, r \in T, \end{aligned} \tag{12}$$

where $\mathcal{K}_0(r)$ is the overall mean effect, $\tau_i(r)$ is the effect of the ith level of the *row factor* A, $\beta_j(r)$ is the effect of the jth level of *column factor* B, $(\tau\beta)_{ij}(r)$ is the effect of the interaction between $\tau_i(r)$ and $\beta_j(r)$. Both factors are assumed to be fixed, and the factor effects are defined as deviations from the overall mean. If nothing more is stated about the decomposition (12), the components of the decomposition are not uniquely defined. Some restrictions over the decomposition are then required (see e.g. Zhang 2013). We set

$$\sum_i \tau_i(r) = \sum_j \beta_j(r) = \sum_i (\tau\beta)_{ij}(r) = \sum_j (\tau\beta)_{ij}(r) = 0.$$

So, hereafter, we limit our discussion to equi-replicated orthogonal ANOVA. We are then interested in testing equality of factor effects (hereafter *treatments*), i.e. that there are no treatment effects in both row treatments

$$\begin{aligned} &\mathscr{H}_0^A : \tau_1(r) = \cdots = \tau_a(r) = 0, r \in T, \\ &\mathscr{H}_1^A : \tau_i(r) \neq 0, \text{ for some } i, \text{ and for some } r \in T, \end{aligned} \tag{13a}$$

and column treatments

$$\begin{aligned} &\mathscr{H}_0^B : \beta_1(r) = \cdots = \beta_b(r) = 0, r \in T, \\ &\mathscr{H}_1^B : \beta_j(r) \neq 0, \text{ for some } j, \text{ and for some } r \in T, \end{aligned} \tag{13b}$$

as well as testing if the main effects are simultaneously zero,

$$\begin{aligned}\mathscr{H}_0^{AB} &: \tau_i(r) = \beta_j(r) = 0 \text{ for all } i,\ j,\ \text{and } r \in T,\\ \mathscr{H}_1^{AB} &: \text{at least one } \tau_i(r) \text{ or } \beta_j(r) \neq 0,\ \text{for some } r \in T.\end{aligned} \tag{13c}$$

Finally, we could be interested in determining whether row and column factors interact, so testing

$$\begin{aligned}\mathscr{H}_0^{I} &: (\tau\beta)_{ij}(r) = 0 \quad \text{for all } i,\ j,\ \text{and for } r \in T,\\ \mathscr{H}_1^{I} &: \text{at least one } (\tau\beta)_{ij}(r) \neq 0,\ \text{for some } r \in T.\end{aligned} \tag{13d}$$

The estimators of cell mean and variance functions are well-defined whenever $c > 1$. We consider the same pooled estimators defined in Sect. 2.2 including factors and their levels so that we have cell weighted mean and covariance functions given by

$$\bar{K}_{ij\cdot}(r) = \frac{1}{\omega_{ij\cdot}} \sum_{k=1}^{c} \omega_{ijk} \hat{K}_{ijk}(r), \quad i = 1, \ldots, a, \quad j = 1, \ldots, b, \tag{14}$$

and

$$\hat{\sigma}_{ij}(r) = \quad \frac{1}{c-1} \sum_{i=1}^{c} \left[\hat{K}_{ijk}(r) - \bar{K}_{ij\cdot}(r) \right]^2, \tag{15}$$

where the weights ω_{ijk} are defined as in Eq. (5), and the number of points per pattern is denoted by n_{ijk}, where k is the individual within the ij cell (sample) and $i = 1, \ldots, a$ and $j = 1, \ldots, b$, and $\omega_{ij\cdot} = \sum_{k=1}^{c} n_{ijk}(n_{ijk} - 1)$. As in the classical ANOVA two-way analysis, we define $\bar{K}_{i\cdot\cdot}$, $\bar{K}_{\cdot j\cdot}$ and $\bar{K}_{\cdot\cdot\cdot}$ as the corresponding row, column, and grand weighted average K-functions. Thus,

$$\begin{aligned}\bar{K}_{i\cdot\cdot}(r) &= \frac{1}{\omega_{i\cdot\cdot}} \sum_{j=1}^{b} \omega_{ij\cdot} \bar{K}_{ij\cdot}(r), \quad i = 1, \ldots, a,\\ \bar{K}_{\cdot j\cdot}(r) &= \frac{1}{\omega_{\cdot j\cdot}} \sum_{i=1}^{a} \omega_{ij\cdot} \bar{K}_{ij\cdot}(r), \quad j = 1, \ldots, b,\\ \bar{K}_{\cdot\cdot\cdot}(r) &= \frac{1}{\omega_{\cdot\cdot\cdot}} \sum_{i=1}^{a} \sum_{j=1}^{b} \omega_{ij\cdot} \bar{K}_{ij\cdot}(r),\end{aligned} \tag{16}$$

where

$$\omega_{i\cdot\cdot} = \sum_{j=1}^{b} \omega_{ij\cdot}, \omega_{\cdot j\cdot} = \sum_{i=1}^{a} \omega_{ij\cdot} \text{ and } \omega_{\cdot\cdot\cdot} = \sum_{i=1}^{a} \sum_{j=1}^{b} \omega_{ij\cdot}. \tag{17}$$

From (16), the estimators of the general mean, main and interaction effects are then

$$\begin{aligned}
\hat{\mathcal{K}}_0(r) &= \bar{K}_{\cdots}(r),\\
\hat{\tau}_i(r) &= \bar{K}_{i\cdot\cdot}(r) - \bar{K}_{\cdots}(r),\\
\hat{\beta}_j(r) &= \bar{K}_{\cdot j\cdot}(r) - \bar{K}_{\cdots}(r),\\
\widehat{(\tau\beta)}_{ij}(r) &= \bar{K}_{ij\cdot}(r) - \bar{K}_{i\cdot\cdot}(r) - \bar{K}_{\cdot j\cdot}(r) + \bar{K}_{\cdots}(r).
\end{aligned}$$

Analogous to the classical functional data analysis, consider some fixed $r \in T$ and let $\mathrm{SST}(r)$ be the pointwise total-sum-of-squares, $\mathrm{SSA}(r)$, $\mathrm{SSB}(r)$ are the main-effect pointwise sum-of-squares, respectively, and let $\mathrm{SSI}(r)$ be the interaction-effect pointwise sum-of-squares. Finally, let $\mathrm{SSE}(r)$ denote the pointwise sum-of-squares due to errors. Following the classical balanced two-way ANOVA, we can define the following estimators:

$$\begin{aligned}
\mathrm{SSA}(r) &= bc\sum_{i=1}^{a}[\bar{K}_{i\cdot\cdot}(r) - \bar{K}_{\cdots}(r)]^2 = bc\sum_{i=1}^{a}\hat{\tau}_i^2(r),\\
\mathrm{SSB}(r) &= ac\sum_{j=1}^{b}[\bar{K}_{\cdot j\cdot}(r) - \bar{K}_{\cdots}(r)]^2 = ac\sum_{j=1}^{b}\hat{\beta}_j^2(r),\\
\mathrm{SSI}(r) &= \sum_{i=1}^{a}\sum_{j=1}^{b}[\bar{K}_{ij\cdot}(r) - \bar{K}_{i\cdot\cdot}(r) - \bar{K}_{\cdot j\cdot}(r) + \bar{K}_{\cdots}(r)]^2 8 = c\sum_{i=1}^{a}\sum_{j=1}^{b}\widehat{(\tau\beta)}_{ij}^2(r),\\
\mathrm{SSE}(r) &= \sum_{i=1}^{a}\sum_{j=1}^{b}\sum_{k=1}^{c}\left[\hat{K}_{ijk}(r) - \bar{K}_{ij\cdot}(r)\right]^2 = (c-1)\sum_{i=1}^{a}\sum_{j=1}^{b}\hat{\sigma}_{ij}^2(r).
\end{aligned} \tag{18}$$

The corresponding L^2-norm-based test statistics for our null hypotheses $\mathscr{H}_0^A$, $\mathscr{H}_0^B$, $\mathscr{H}_0^{AB}$ and $\mathscr{H}_0^I$, respectively, are

$$\begin{aligned}
D^A &= \int_T \frac{\mathrm{SSA}_n(r)}{r^2}\mathrm{d}r = bc\sum_{i=1}^{a}\int_T \frac{\hat{\tau}_i^2(r)}{r^2}\mathrm{d}r,\\
D^B &= \int_T \frac{\mathrm{SSB}_n(r)}{r^2}\mathrm{d}r = ac\sum_{j=1}^{b}\int_T \frac{\hat{\beta}_j^2(r)}{r^2}\mathrm{d}r,\\
D^{AB} &= \int_T \frac{1}{r^2}[\mathrm{SSA}(r) + \mathrm{SSB}(r)]\mathrm{d}r = D^A + D^B \quad \text{and}\\
D^I &= \int_T \frac{\mathrm{SSI}_n(r)}{r^2}\mathrm{d}r = c\sum_{i=1}^{a}\sum_{j=1}^{b}\int_T \frac{\widehat{(\tau\beta)}_{ij}^2(r)}{r^2}\mathrm{d}r.
\end{aligned} \tag{19}$$

Similarly, for the Fisher-test-type statistics for $\mathscr{H}_0^A$, $\mathscr{H}_0^B$, $\mathscr{H}_0^{AB}$ and $\mathscr{H}_0^I$, respectively, we have

$$\begin{aligned} F^A &= \frac{\int_T \mathrm{SSA}(r)\mathrm{d}r/(a-1)}{\int_T \mathrm{SSE}(r)\mathrm{d}r/(ab(c-1))}, \\ F^B &= \frac{\int_T \mathrm{SSB}(r)\mathrm{d}r/(b-1)}{\int_T \mathrm{SSE}(r)\mathrm{d}r/(ab(c-1))}, \\ F^{AB} &= \frac{\int_T [\mathrm{SSA}(r)+\mathrm{SSB}(r)]\,\mathrm{d}r/(a+b-2)}{\int_T \mathrm{SSE}(r)\mathrm{d}r/(ab(c-1))}, \\ F^I &= \frac{\int_T \mathrm{SSI}(r)\mathrm{d}r/\left((a-1)(b-1)\right)}{\int_T \mathrm{SSE}(r)\mathrm{d}r/(ab(c-1))}. \end{aligned} \tag{20}$$

Remark 1 Note that the entire previous theoretical approach can be reproduced in identical conditions by replacing Ripley's K-function with its respective weighted mark version (see e.g. Baddeley et al. 2015). Undoubtedly, the variance, in that case, becomes increasingly difficult to be controlled since the distribution of the marks implies an additional source of variation. However, the inclusion of marks constitutes a much more realistic treatment whenever the marks and locations are dependent. See further comments in Sect. 5.

3.3 Random permutation tests

The null distribution of our test statistics is not analytically tractable in any of the cases. We assume that the observed K-functions come from the statistical model (11). In order to determine the null distribution of the test statistics, some authors use the so-called *bootstrap based on residuals* method. This method was proposed by Efron (1979), and has been applied in the point process context by e.g. Diggle et al. (1991), Wilson (1998) and Ramón et al. (2016).

In classical ANOVA designs, many permutation strategies can be applied for testing individual terms. Anderson and Braak (2003) provides a complete guide to building accurate and approximate permutation strategies for all terms in a two-way ANOVA. Following this motivation, we consider inference by choosing several types of exchangeable units, i.e. quantities that can be the raw observations or other, and that can fall in either group under the null hypothesis. We draw random permutations of these exchangeable units to obtain an empirical p-value.

We provide results of Monte Carlo simulations for the empirical level and the power of our tests. We consider some standard cases, namely Poisson (complete spatial random model), cluster (aggregation model) and inhibition (regular model) processes.

We set an equi-replicated design with two factors with three levels each one, equal observation windows (unit square window $[0,1] \times [0,1]$) and small sample sizes per level of each factor $c = 6$. We are interested in those situations in which the overall hypotheses hold: the underlying point processes have the same K-function, meaning they have the same approximated spatial distribution and such distribution is not affected by the levels of factors. Recall that we are investigating second-order

Table 1 Arrangement of independent configurations of cell intensities in a two-way ANOVA design where responses are Poisson point patterns

Homoscedastic configurations		Heteroscedastic configurations	
SConf.1	$\lambda = \begin{pmatrix} 50 & 50 & 50 \\ 50 & 50 & 50 \\ 50 & 50 & 50 \end{pmatrix}$	DConf.1	$\lambda = \begin{pmatrix} 50 & 50 & 50 \\ 100 & 100 & 100 \\ 150 & 150 & 150 \end{pmatrix}$
SConf.2	$\lambda = \begin{pmatrix} 100 & 100 & 100 \\ 100 & 100 & 100 \\ 100 & 100 & 100 \end{pmatrix}$	DConf.2	$\lambda = \begin{pmatrix} 50 & 100 & 150 \\ 50 & 100 & 150 \\ 50 & 100 & 150 \end{pmatrix}$
SConf.3	$\lambda = \begin{pmatrix} 150 & 150 & 150 \\ 150 & 150 & 150 \\ 150 & 150 & 150 \end{pmatrix}$	DConf.3	$\lambda = \begin{pmatrix} 60 & 120 & 180 \\ 80 & 140 & 200 \\ 100 & 160 & 220 \end{pmatrix}$

Each matrix represents a configuration of intensities for the patterns within each cell (treatment)

behaviour, i.e. the patterns may have different intensities. The integrals are numerically approximated by using the trapezoidal rule. For the integration upper bound, we take some inspiration on Hahn (2012) who investigated, by simulation, a permutation test based on an integrated version of Welch's t-test statistic, and found that tests with upper integration limit of $r_0 = 0.15$, were overall most powerful. We perform each value through 1000 random permutations of observed stationary K-functions estimated by using Ripley's edge-correction. We consider several scenarios to the null hypothesis in order to verify the performance of the test under homoscedastic and heteroscedastic cases.

3.3.1 Models

Poisson model We first consider complete spatial random patterns (**Poisson** patterns) with some configurations of homoscedasticity and heteroscedasticity given by the intensity of the process in each cell of the design, such configurations are shown in Table 1. Notice that we arrange the different values of the intensity for each cell (each treatment) in a matrix, so a component ij of such matrix represents the intensity of the cell ij (six homogeneous point patterns with that intensity).

Hard-core and cluster models We also consider point patterns from *Matérn hard-core* and *cluster* point processes (see, e.g. Chiu et al. 2013 and references therein) with parameters leading to different degrees of regularity or clustering. Both types of point processes come from a parent Poisson point process. In this case, we use a Matérn hard-core obtained by dependent thinning. The points are first marked with random numbers (independent, and identically distributed); a particular point is dropped whenever it has a neighbour (separated at most a distance h, known as hard-core distance) with a smaller mark. This type of process is known as Matérn model II [see, e.g. Baddeley et al. (2015)]. Note that the intensity of the hard-core point processes is a function of their inhibition distance and the intensity of the parent process. Therefore, fixing an underline Poisson process for the parents, the intensities of the hard-core processes are the same provided their inhibition distances do not change. On the other hand,

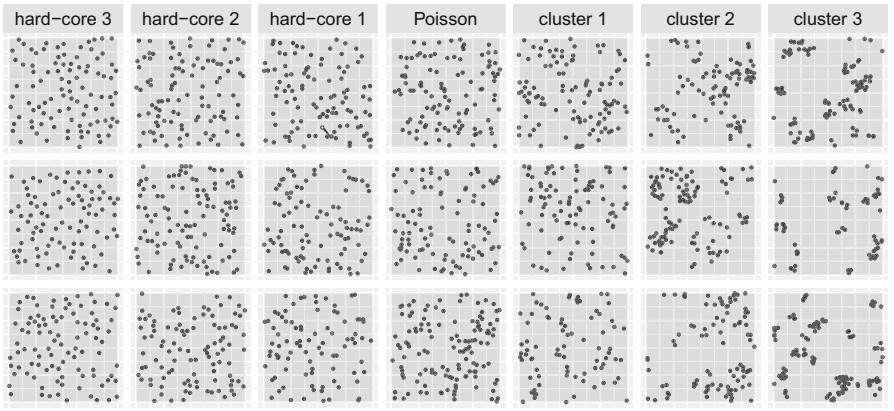

Fig. 4 Sets of three independent realisations of Matérn hard-core, Poisson and Matérn cluster point processes on the unit square. Model parameters: hard-core radius (1) $h = 0.01$, (2) $h = 0.03$ and (3) $h = 0.05$; mean number μ of points per cluster and cluster radius r (1) $\mu = 1, r = 0.1$, (2) $\mu = 4, r = 0.1$, (3) $\mu = 4, r = 0.05$

a Matérn's cluster point process consists of independent clusters of daughter points around each parent point. The numbers of daughter points per cluster are Poisson distributed with mean μ, and the points are independently uniformly scattered in the ball with centre in the parent point and radius r. The parent points are not included in the observed point pattern. Some realisations of these two processes and CSR are shown in Fig. 4.

3.3.2 Permutation test approach

Following Anderson and Braak (2003), we adopt a permutation strategy consisting of permuting weighted residuals (exchangeable units) instead of a combination of residuals and means. In other words, permuted residuals are plugged-in to the Fisher-based statistics after rescaling them. We propose to define the full-model weighted residuals $\hat{R}_{ijk}(r)$ as

$$\hat{R}_{ijk}(r) = \sqrt{n_{ijk}(n_{ijk}-1)}\left[\hat{K}_{ijk}(r) - \bar{K}_{ij\cdot}(r)\right], \quad i = 1,\ldots,a, \quad j = 1,\ldots,b, \quad k = 1,\ldots c. \tag{21}$$

Note that we cannot construct an exact test since the assumption of exchangeability is not strictly satisfied, that is, the residuals are weakly correlated and the correction factor $\sqrt{n_{ijk}(n_{ijk}-1)}$ is motivated by the asymptotic approximation of the variance of Ripley's K-function for Poisson point patterns, where the number of points has been observed (Ripley 1988). We can calculate the statistics by using the residuals and generate a large number of random permutations to obtain an empirical approximation of the $(1-\alpha)$-percentiles of our test statistics.

For the interaction effect, we also consider the saturated-model residuals proposed by Wilson (1998) and applied by Ramón et al. (2016). Indeed, we subtract out the

main effects and the weighted version of the residuals gives

$$\hat{R}^{\dagger}_{ijk}(r) = \sqrt{n_{ijk}(n_{ijk}-1)}\left[\hat{K}_{ijk}(r) - \bar{K}_{i\cdot\cdot}(r) - \bar{K}_{\cdot j\cdot}(r) + \bar{K}_{\cdot\cdot\cdot}(r)\right], \quad i = 1,\ldots,a, \quad j = 1,\ldots,b, \quad k = 1,\ldots c. \tag{22}$$

These residuals are meant to attempt to control for main effects and asymptotically approach an exact test (where the residuals hold the exchangeability assumption) because, although SSA and SSB are not kept constant, variability due to A and B is estimated and removed by subtracting weighted means.

We go further and propose some residuals to study the main effects. These reduced-model residuals have been motivated by those suggested by Diggle et al. (1991), although they have never been used in this context, not even in the one-way case. The residuals are given by

$$\hat{R}^{\dagger A}_{ijk}(r) = \sqrt{n_{ijk}(n_{ijk}-1)}\left[\hat{K}_{ijk}(r) - \bar{K}_{i\cdot\cdot}(r)\right], \quad i = 1,\ldots,a, \quad j = 1,\ldots,b, \quad k = 1,\ldots c, \tag{23}$$

for the row effect, and

$$\hat{R}^{\dagger B}_{ijk}(r) = \sqrt{n_{ijk}(n_{ijk}-1)}\left[\hat{K}_{ijk}(r) - \bar{K}_{\cdot j\cdot}(r)\right], \quad i = 1,\ldots,a, \quad j = 1,\ldots,b, \quad k = 1,\ldots c, \tag{24}$$

for the column effect.

Note that we follow the implicit recommendation in Baddeley et al. (2015, p. 421) of rescaling the residuals with a factor $\sqrt{n_{ijk}(n_{ijk}-1)}$. For the particular case of resampling K-functions, the suggestion goes back to Hahn (2012), where they proved that the proper weights are the number of points n_{ijk} (roughly our weights) rather than their square root.

3.3.3 Significance level under the null hypothesis

The available methodologies for the analysis of variance in the context of point processes are given by using D-type statistics, given in Eq. (19), whose null distribution is obtained by permuting residuals proportional to $\hat{R}_{ijk}(r)$ for all effects (Wilson 1998) or permuting residuals proportional to $\hat{R}^{\dagger}_{ijk}(r)$ for interaction effects (Ramón et al. 2016). Therefore, we first study the empirical distribution of D-type statistics by permuting residuals $\hat{R}_{ijk}(r)$ and by using the simplest scenario (Poisson) with configurations given in Table 1. We set $\alpha = 0.01, 0.05, 0.10$ as nominal significance levels and estimate the rejection rates for each case. The results are shown in Table 2. Unfortunately, these test statistics show a poor performance (liberality) in homoscedastic cases. As expected, they are also not doing better in heteroscedastic ones. From now on, we study our proposed F-statistics by using the residuals for testing each effect.

Table 2 Rejection rates from replicated simulations of the null hypothesis of no differences amongst the samples of K-functions of two factors with three levels using test statistics given in Eq. (19)

	D	Nominal sig. level				D	Nominal sig. level		
		0.01	0.05	0.10			0.01	0.05	0.10
SConf.1	D^A	0.034	0.099	0.178***	DConf.1	D^A	0.060	0.152	0.232***
	D^B	0.024	0.093	0.154***		D^B	0.020	0.083	0.138***
	D^{AB}	0.041	0.131	0.208***		D^{AB}	0.060	0.154	0.238***
	D^I	0.039	0.124	0.189***		D^I	0.034	0.119	0.210***
SConf.2	D^A	0.028	0.097	0.164***	DConf.2	D^A	0.022	0.065	0.123***
	D^B	0.029	0.088	0.173***		D^B	0.055	0.162	0.268***
	D^{AB}	0.046	0.121	0.197***		D^{AB}	0.059	0.172	0.266***
	D^I	0.037	0.123	0.203***		D^I	0.047	0.136	0.202***
SConf.3	D^A	0.022	0.108	0.175***	DConf.3	D^A	0.029	0.079	0.133***
	D^B	0.034	0.097	0.160***		D^B	0.030	0.127	0.218***
	D^{AB}	0.045	0.118	0.198***		D^{AB}	0.039	0.140	0.231***
	D^I	0.047	0.125	0.210***		D^I	0.054	0.146	0.251***

The scenarios indicated in the left columns are shown in Table 1. Exchangeable units for a test were the residuals given in Eq. (21). Values lying outside the 95% confidence interval for type I error (which has a binomial distribution with parameters $n = 1000$, $p = 0.01, 0.05$ and 0.1) are indicated with ***, **, * in the case of violation of the three, two or one nominal levels respectively, and with no symbol in case of no violation

Table 3 shows the performance for the homoscedastic and heteroscedastic Poisson cases, and Table 4 shows the performance for the specific cluster and hard-core models using the residuals given in Eq. (21).

Tables 3 and 4 show much better performance even in heteroscedastic cases. It is important to highlight the good performance of the test statistic F^I that measures the interaction effect. This statistic is probably the most important in an ANOVA two-way design because if the interaction is significant, the interpretation of the individual effects of the factors becomes incomplete and misleading. Going further with the interaction effect, the performance of the test statistic F^I, by using residuals (22), is shown in Table 5.

Once again, the test statistic F^I shows a satisfactory performance (even in the case of heteroscedasticity). This shows that, for the interaction, both types of residuals are efficient and robust against a moderate violation of the equality of variances.

By using the same simulation scheme, we study the reduced-model residuals (Eqs. 23, 24) that in theory are the most adequate to test the main effects in ANOVA two-way designs (Anderson and Braak 2003). The performance is shown in Table 6.

Interestingly, reduced-model residuals (Eqs. 23, 24) do not outperform the full-model residuals when using Fisher-test-type statistics to test the significance of the main effects.

Table 3 Rejection rates from replicated simulations of the null hypothesis of no differences amongst the samples of K-functions

	F	Nominal sig. level			F		Nominal sig. level		
		0.01	0.05	0.10			0.01	0.05	0.10
SConf.1	F^A	0.011	0.047	0.089	DConf.1	F^A	0.015	0.086	0.152**
	F^B	0.006	0.037	0.086		F^B	0.008	0.037	0.069**
	F^{AB}	0.006	0.044	0.094		F^{AB}	0.021	0.077	0.137***
	F^I	0.007	0.043	0.084		F^I	0.008	0.053	0.104
SConf.2	F^A	0.011	0.041	0.084	DConf.2	F^A	0.008	0.044	0.082
	F^B	0.012	0.048	0.096		F^B	0.021	0.088	0.161***
	F^{AB}	0.011	0.043	0.083		F^{AB}	0.014	0.083	0.148**
	F^I	0.009	0.042	0.095		F^I	0.010	0.057	0.110
SConf.3	F^A	0.009	0.050	0.101	DConf.3	F^A	0.011	0.038	0.078*
	F^B	0.014	0.051	0.087		F^B	0.010	0.063	0.118
	F^{AB}	0.008	0.048	0.094		F^{AB}	0.008	0.059	0.113
	F^I	0.020	0.054	0.112*		F^I	0.009	0.063	0.118

Fisher-test-type statistics are used by including the degrees of freedom within the statistic. Exchangeable units for tests were the residuals $\hat{R}_{ijk}(r)$ given in Eq. (21). Values are indicated as in Table 2

3.3.4 Power of the tests

Analysing the power of ANOVA (even in the classical case) is far from being a simple task. The problem is that there are infinite possibilities to get away from the null hypotheses, and each one of those infinite differences implies a different power. The problem comes from trying to compare several groups according to all the levels of the factors and replicates.

The K-function is quite sensitive to the aggregation parameters of the underlying point process. For example, all Poisson processes have the same theoretical K-function (πr^2 in the planar case). So, we can move away from the null hypothesis by systematically increasing or decreasing these parameters. Our most general alternative hypothesis is that the levels of the factors and the interaction between them, affect in a significant way the K-functions of the observed point patterns.

In a Matérn-cluster process (as a particular case of a Neyman-Scott process) the K-function depends on the parents' intensity and the cluster radius (Diggle 2013). Therefore, we could quickly establish structural differences between Matérn processes through the variation of these two parameters. On the other hand, in a Matérn hard-core process, the K-function depends on both the intensity of the proposal-points and the inhibition distance (Cressie 1993). So, again, we could fix structural differences through the modification of these two parameters.

Consider a set of 6 Matérn cluster point patterns with $\kappa = 25$, $\mu = 4$, and radii 0.1, this configuration will correspond to the combination of levels ($A = 1$, $B = 1$); then for ($A = 2$, $B = 2$), consider another set of 6 Matérn cluster point patterns with the same intensity but radii 0.3 and for ($A = 3$, $B = 3$) the radii shall be 0.5.

Table 4 Performance of the test for **cluster** (left) and **hard-core** (right) models whose parameters are given in the left columns

	F	Nominal sig. level				F	Nominal sig. level		
		0.01	0.05	0.10			0.01	0.05	0.10
$\mu = 1, r = 0.1$	F^A	0.009	0.061	0.108	$h = 0.05$	F^A	0.009	0.044	0.096
$\kappa = 100$	F^B	0.011	0.049	0.091		F^B	0.010	0.047	0.102
	F^{AB}	0.016	0.061	0.086		F^{AB}	0.008	0.047	0.101
	F^I	0.013	0.046	0.098		F^I	0.014	0.046	0.095
$\mu = 4, r = 0.1$	F^A	0.008	0.052	0.115	$h = 0.02$	F^A	0.010	0.043	0.097
$\kappa = 100$	F^B	0.009	0.053	0.110		F^B	0.006	0.040	0.093
	F^{AB}	0.013	0.058	0.115		F^{AB}	0.012	0.046	0.094
	F^I	0.016	0.057	0.107		F^I	0.010	0.038	0.090
$\mu = 4, r = 0.05$	F^A	0.015	0.065	0.113*					
$\kappa = 100$	F^B	0.010	0.057	0.108					
	F^{AB}	0.017	0.069	0.114**					
	F^I	0.011	0.061	0.104					

Exchangeable units for a test are the residuals $\hat{R}_{ijk}(r)$ given in Eq. (21). Values are indicated as in Table 2

Table 5 Rejection rates from replicated simulations of the true null hypothesis of no interaction between factors A and B by using residuals $\hat{R}^{\dagger}_{ijk}(r)$ given in Eq. (22)

Poisson					Cluster				
	F	Nominal sig. level				F	Nominal sig. level		
		0.01	0.05	0.10			0.01	0.05	0.10
SConf.1	F^I	0.008	0.042	0.094	$\mu = 1, r = 0.1, \kappa = 100$	F^I	0.008	0.042	0.098
SConf.2	F^I	0.012	0.048	0.097	$\mu = 4, r = 0.1, \kappa = 25$	F^I	0.011	0.047	0.091
SConf.3	F^I	0.012	0.054	0.095	$\mu = 4, r = 0.05, \kappa = 25$	F^I	0.013	0.047	0.094
DConf.1	F^I	0.011	0.052	0.103	Hard-core				
DConf.2	F^I	0.016	0.049	0.088	$h = 0.05$	F^I	0.006	0.048	0.097
DConf.3	F^I	0.010	0.049	0.088	$h = 0.02$	F^I	0.015	0.055	0.105

Three null models are considered: homogeneous **Poisson** (left), **cluster** (right-up) and **hard-core** (right-down) as underlying processes. Values are indicated as in Table 2

Table 6 Rejection rates from replicated simulations of the true null hypothesis of no main effects in the samples of K-functions

Poisson					Cluster				
	F	Nominal sig. level				F	Nominal sig. level		
		0.01	0.05	0.10			0.01	0.05	0.10
SConf.1	F^A	0.008	0.046	0.087	$\mu = 1, r = 0.1$	F^A	0.013	0.058	0.104
	F^B	0.012	0.051	0.096	$\kappa = 100$	F^B	0.010	0.047	0.082
	F^{AB}	0.011	0.054	0.094		F^{AB}	0.014	0.054	0.102
SConf.2	F^A	0.008	0.051	0.108	$\mu = 4, r = 0.1$	F^A	0.008	0.040	0.075*
	F^B	0.014	0.046	0.095	$\kappa = 100$	F^B	0.009	0.044	0.082
	F^{AB}	0.007	0.047	0.102		F^{AB}	0.008	0.037	0.077*
SConf.3	F^A	0.009	0.051	0.098	$\mu = 4, r = 0.05$	F^A	0.013	0.048	0.089
	F^B	0.013	0.044	0.092	$\kappa = 100$	F^B	0.009	0.044	0.088
	F^{AB}	0.014	0.052	0.096		F^{AB}	0.007	0.057	0.094
DConf.1	F^A	0.032	0.095	0.163***	Hard-core				
	F^B	0.005	0.027	0.065**	$h = 0.05$	F^A	0.004	0.043	0.091
	F^{AB}	0.031	0.087	0.143***		F^B	0.009	0.049	0.096
DConf.2	F^A	0.008	0.034	0.069**		F^{AB}	0.010	0.041	0.095
	F^B	0.027	0.097	0.163***	$h = 0.02$	F^A	0.014	0.057	0.100
	F^{AB}	0.029	0.091	0.151***		F^B	0.017	0.059	0.099*
DConf.3	F^A	0.008	0.043	0.078*		F^{AB}	0.016	0.060	0.110
	F^B	0.018	0.063	0.127**					
	F^{AB}	0.013	0.061	0.115					

Three null models are considered: homogeneous **Poisson** (left), **cluster** (right-up) and **hard-core** (right-down) as underlying processes. Exchangeable units are the reduced-model residuals $\hat{R}^{\dagger A}_{ijk}(r)$, $\hat{R}^{\dagger B}_{ijk}(r)$ (Eqs. 23, 24). Values are indicated as in Table 2

Table 7 Configurations of systematic departures from null hypotheses of no interaction between factors in ANOVA two-way design

Cluster configurations		Hard-Core configurations	
$\mathbf{r}_1^{AB} = \begin{pmatrix} 0 & & \\ & 0.002 & \\ & & 0.004 \end{pmatrix}$	$+\phi_c\mathbf{J}_3$	$\mathbf{h}_1^{AB} = \begin{pmatrix} 0 & & \\ & 0.002 & \\ & & 0.004 \end{pmatrix}$	$+\phi_i\mathbf{J}_3$
$\mathbf{r}_2^{AB} = \begin{pmatrix} 0 & & \\ & 0.1 & \\ & & 0.2 \end{pmatrix}$	$+\phi_c\mathbf{J}_3$	$\mathbf{h}_2^{AB} = \begin{pmatrix} 0 & & \\ & 0.005 & \\ & & 0.01 \end{pmatrix}$	$+\phi_i\mathbf{J}_3$
$\mathbf{r}_3^{AB} = \begin{pmatrix} 0 & & \\ & 0.5 & \\ & & 1.0 \end{pmatrix}$	$+\phi_c\mathbf{J}_3$	$\mathbf{h}_3^{AB} = \begin{pmatrix} 0 & & \\ & 0.015 & \\ & & 0.03 \end{pmatrix}$	$+\phi_i\mathbf{J}_3$
$\mathbf{r}_1^{B} = \begin{pmatrix} 0 & 0.002 & 0.004 \\ 0 & 0.002 & 0.004 \\ 0 & 0.002 & 0.004 \end{pmatrix}$	$+\phi_c\mathbf{J}_3$	$\mathbf{h}_1^{B} = \begin{pmatrix} 0 & 0.002 & 0.004 \\ 0 & 0.002 & 0.004 \\ 0 & 0.002 & 0.004 \end{pmatrix}$	$+\phi_i\mathbf{J}_3$
$\mathbf{r}_2^{B} = \begin{pmatrix} 0 & 0.1 & 0.2 \\ 0 & 0.1 & 0.2 \\ 0 & 0.1 & 0.2 \end{pmatrix}$	$+\phi_c\mathbf{J}_3$	$\mathbf{h}_2^{B} = \begin{pmatrix} 0 & 0.005 & 0.01 \\ 0 & 0.005 & 0.01 \\ 0 & 0.005 & 0.01 \end{pmatrix}$	$+\phi_i\mathbf{J}_3$
$\mathbf{r}_3^{B} = \begin{pmatrix} 0 & 0.5 & 1.0 \\ 0 & 0.5 & 1.0 \\ 0 & 0.5 & 1.0 \end{pmatrix}$	$+\phi_c\mathbf{J}_3$	$\mathbf{h}_3^{B} = \begin{pmatrix} 0 & 0.015 & 0.03 \\ 0 & 0.015 & 0.03 \\ 0 & 0.015 & 0.03 \end{pmatrix}$	$+\phi_i\mathbf{J}_3$

The parameters of the cluster processes are $\mu \in \{1, 4, 4\}$, $\kappa \in \{100, 25, 25\}$ and $\phi_c \in \{0.1, 0.05\}$. The intensity of the parents for inhibition processes is 200, and $\phi_i \in \{0.005, 0.01, 0.02\}$

For all the remaining combinations of the levels of A and B, assume radii of 0.1. This configuration constrains the K-function to depend on the factors' interaction and allows for measuring the tests' power by using the different residuals. For the case of main effects, we can arrange a configuration where radii increase with rows or columns allowing to measure the power of main effects statistics and residuals. We can summarise such radii configuration in matrices as we do for the level of the tests, for example,

$$\mathbf{r}^{AB} = \begin{pmatrix} 0.1 & & \\ & 0.3 & \\ & & 0.5 \end{pmatrix} + \phi_c\mathbf{J}_3, \qquad \mathbf{r}^{A} = \begin{pmatrix} 0 & 0.2 & 0.4 \\ 0 & 0.2 & 0.4 \\ 0 & 0.2 & 0.4 \end{pmatrix} + \phi_c\mathbf{J}_3, \tag{25}$$

where ϕ_c is a constant representing an initial configuration of radii, i.e. the null hypothesis, and $\mathbf{J}_3$ denotes the 3×3 matrix of ones, so that the remaining matrix means to control the subsequent departures from the null hypothesis. Note that every entry represents an entire cell of 6 point patterns. Also, any alternative hypotheses for rows or columns effects, apply directly over the effects of addition of rows and columns (note that in this case, the effects of rows and columns are not simultaneously zero). To study the power of the test statistic for the interaction effects, we fix a set of configurations given in Table 7.

The results of the simulations for the power of the interaction and main effects statistics are shown in Table 8.

Table 8 Empirical power for interaction (F^I) and main effect statistics (F^B, as the parameters of the models grow by columns) when the underlying point processes are cluster and hard-core with parameters given in Table 7

Cluster configurations						Hard-core configurations					
Conf.	Residual	(μ, κ, ϕ_c)	Nominal sig. level			Conf.	Residual	ϕ_i	Nominal sig. level		
			0.01	0.05	0.1				0.01	0.05	0.1
$\mathbf{r}_1^{AB}$	$\hat{R}_{ijk}(r)$	(1, 100, 0.1)	0.011	0.054	0.108	$\mathbf{h}_1^{AB}$	$\hat{R}_{ijk}(r)$	0.005	0.011	0.052	0.102
		(4, 25, 0.1)	0.014	0.043	0.091			0.01	0.014	0.064	0.106
		(4, 25, 0.05)	0.007	0.044	0.094			0.02	0.023	0.072	0.132
	$\hat{R}_{ijk}^{\dagger}(r)$	(1, 100, 0.1)	0.014	0.050	0.092		$\hat{R}_{ijk}^{\dagger}(r)$	0.005	0.007	0.038	0.101
		(4, 25, 0.1)	0.011	0.044	0.095			0.01	0.016	0.071	0.129
		(4, 25, 0.05)	0.009	0.034	0.082			0.02	0.014	0.067	0.131
$\mathbf{r}_2^{AB}$	$\hat{R}_{ijk}(r)$	(1, 100, 0.1)	0.056	0.217	0.365	$\mathbf{h}_2^{AB}$	$\hat{R}_{ijk}(r)$	0.005	0.015	0.079	0.138
		(4, 25, 0.1)	0.361	0.710	0.856			0.01	0.019	0.084	0.172
		(4, 25, 0.05)	0.624	0.903	0.966			0.02	0.047	0.164	0.310
	$\hat{R}_{ijk}^{\dagger}(r)$	(1, 100, 0.1)	0.058	0.203	0.364		$\hat{R}_{ijk}^{\dagger}(r)$	0.005	0.009	0.057	0.130
		(4, 25, 0.1)	0.326	0.700	0.856			0.01	0.013	0.082	0.177
		(4, 25, 0.05)	0.633	0.911	0.964			0.02	0.041	0.181	0.301
$\mathbf{r}_3^{AB}$	$\hat{R}_{ijk}(r)$	(1, 100, 0.1)	0.140	0.409	0.587	$\mathbf{h}_3^{AB}$	$\hat{R}_{ijk}(r)$	0.005	0.655	0.953	0.989
		(4, 25, 0.1)	0.779	0.952	0.988			0.01	0.973	1.000	1.000
		(4, 25, 0.05)	0.941	0.989	0.998			0.02	1.000	1.000	1.000
	$\hat{R}_{ijk}^{\dagger}(r)$	(1, 100, 0.1)	0.099	0.393	0.588		$\hat{R}_{ijk}^{\dagger}(r)$	0.005	0.667	0.955	0.991
		(4, 25, 0.1)	0.754	0.961	0.987			0.01	0.968	1.000	1.000
		(4, 25, 0.05)	0.924	0.988	0.995			0.02	1.000	1.000	1.000

Table 8 continued

Cluster configurations						Hard-core configurations					
Conf.	Residual	(μ, κ, ϕ_c)	Nominal sig. level			Conf.	Residual	ϕ_i	Nominal sig. level		
			0.01	0.05	0.1				0.01	0.05	0.1
$\mathbf{r}_1^B$	$\hat{R}_{ijk}(r)$	(1, 100, 0.1)	0.017	0.052	0.089	$\mathbf{h}_1^B$	$\hat{R}_{ijk}(r)$	0.005	0.010	0.054	0.112
		(4, 25, 0.1)	0.014	0.047	0.098			0.01	0.018	0.070	0.128
		(4, 25, 0.05)	0.007	0.047	0.101			0.02	0.053	0.137	0.233
	$\hat{R}_{ijk}^{\dagger B}(r)$	(1, 100, 0.1)	0.009	0.056	0.112		$\hat{R}_{ijk}^{\dagger B}(r)$	0.005	0.022	0.072	0.138
		(4, 25, 0.1)	0.009	0.063	0.110			0.01	0.026	0.096	0.182
		(4, 25, 0.05)	0.011	0.050	0.090			0.02	0.075	0.226	0.352
$\mathbf{r}_2^B$	$\hat{R}_{ijk}(r)$	(1, 100, 0.1)	0.866	0.957	0.981	$\mathbf{h}_2^B$	$\hat{R}_{ijk}(r)$	0.005	0.037	0.136	0.213
		(4, 25, 0.1)	1.000	1.000	1.000			0.01	0.106	0.305	0.441
		(4, 25, 0.05)	1.000	1.000	1.000			0.02	0.546	0.813	0.912
	$\hat{R}_{ijk}^{\dagger B}(r)$	(1, 100, 0.1)	0.952	0.989	0.997		$\hat{R}_{ijk}^{\dagger B}(r)$	0.005	0.100	0.298	0.441
		(4, 25, 0.1)	1.000	1.000	1.000			0.01	0.371	0.651	0.782
		(4, 25, 0.05)	1.000	1.000	1.000			0.02	0.948	0.994	0.997
$\mathbf{r}_3^B$	$\hat{R}_{ijk}(r)$	(1, 100, 0.1)	0.998	1.000	1.000	$\mathbf{h}_3^B$	$\hat{R}_{ijk}(r)$	0.005	1.000	1.000	1.000
		(4, 25, 0.1)	1.000	1.000	1.000			0.01	1.000	1.000	1.000
		(4, 25, 0.05)	1.000	1.000	1.000			0.02	1.000	1.000	1.000
	$\hat{R}_{ijk}^{\dagger B}(r)$	(1, 100, 0.1)	1.000	1.000	1.000		$\hat{R}_{ijk}^{\dagger B}(r)$	0.005	1.000	1.000	1.000
		(4, 25, 0.1)	1.000	1.000	1.000			0.01	1.000	1.000	1.000
		(4, 25, 0.05)	1.000	1.000	1.000			0.02	1.000	1.000	1.000

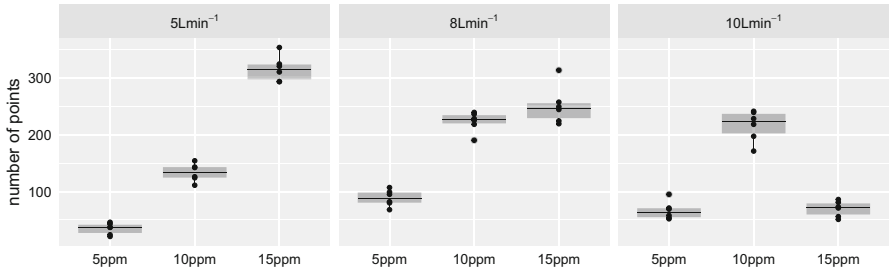

Fig. 5 Box-plots of numbers of bubbles in each level of the two factors. Three panels correspond to the levels of volumetric airflow rate, and the horizontal axis corresponds to frother concentration

Strongly aggregated patterns in the cells (patterns with larger K-functions) are discriminated from weakly aggregated patterns with an approximate probability of 1, and the same happens with strongly regular patterns. As might be expected, as the parameters of the models approach each other, and therefore generate virtually indistinguishable patterns, the power of the tests decreases. Note that we study the power for column main effects, but the results are valid for row main effects.

4 Data analysis

Our practical analysis aims to detect and analyse possible differences due to possible factor effects, in both the densities and the point patterns of bubbles.

Despite the three-dimensional nature of the phenomenon of the floating bubble, the data come from photographs, as explained in Sect. 1. The photographs are the final step of a device (known as *bubble viewer*), built to collect and present bubbles for imaging. This method arises from decades of research on bubble size measurements. It is considered the most efficient method for such an end as the recorded bubbles represent the bubble population in the flotation machine. Furthermore, it accounts for segregation as bubbles rise and spread, and no bubbles are excluded due to their size (see e.g. Chen et al. 2001; Gomez and Finch 2007).

We first carry out an analysis of counts of bubbles using generalised linear modelling. Then, we analyse the possible differences in the spatial point patterns considering all the experimental groups determined by the levels of volumetric airflow rate and frother concentration.

4.1 Poisson log–linear model for the expected cell counts

Since the spatial windows are fixed throughout the experiment, it is sufficient to compare the counts across the levels. Figure 5 shows box-plots of the number of points in each pattern, broken down by the three levels of frother concentration, and faceted by the three levels of volumetric airflow rate. The box-plots in Fig. 5 allow us to suspect that the number of points varies with the levels of the two factors.

We use a quasi-Poisson regression model to deal with possible overdispersion (McCullagh and Nelder 1989; Diggle et al. 1991) with a quasi-likelihood approach. Let us denote as a random variable the count n_{ijk}, and assume that $\mathbb{E}(n_{ijk}) = \mu_{ij}$ and $\mathbb{V}\text{ar}(n_{ijk}) = \phi\mu_{ij}$, where $\phi > 0$ is an overdispersion parameter. We fit the following model

$$\mu_{ij} = \exp\{\beta_0 + \beta_1 i + \beta_2 j + \beta_3 ij\},$$

where β_1 and β_2 are the parameters for the main effects, and β_3 is the parameter for the interaction. The estimated overdispersion parameter is $\hat{\phi} = 2.737$, which is quite high. Such overdispersion can be explained by non-measured covariates, random effects or by non-Poisson variation within bubble point patterns [clustering within the point patterns for instance, see Diggle et al. (1991)].

We test the overall effect of the two factors and their interaction. The Chi-square test indicates statistically significant main effects and interaction between the effects of frother concentration and volumetric airflow rate on the density of the bubbles (Residual Deviance of 123.40, p-value below 0.01) despite the overdispersion.

Furthermore, we have significant positive coefficients for the levels of the factors ($\beta = 1.35$ for 10 ppm, $\beta = 2.21$ for 15 ppm, $\beta = 0.94$ for 8 L min^{-1}, and $\beta = 0.65$ for 10 L min^{-1}; with p-values below 0.001). These are the estimated rate ratios comparing 10 ppm and 15 ppm to 10 ppm, and 8 L min^{-1} and 10 L min^{-1} to 5 L min^{-1}, holding constant the other variables in the model. For example, 15 ppm compared to 5 ppm are expected to have a rate 2.21 times greater for the number of bubbles.

The interaction between the two factors is significant in almost all the level crossings. The combinations 10 ppm and 15 ppm with 8 L min^{-1} ($\beta = -0.42, -1.17$ with p-values below 0.001) as well as 15 ppm with 10 L min^{-1} ($\beta = -2.16$ with a p-value below 0.001), introduce friction in the flotation process, slowing down the increase in bubble counts. The combination 10 ppm with 10 L min^{-1} is not affecting the counts though (p-value of 0.29).

4.2 Spatial distribution of bubble patterns

The 54 point patterns shown in Fig. 3 represent the positions of the bubbles in the flotation experiment described in Sect. 1. The estimated K-functions are shown in Fig. 6.

To measure the variability of the pooled estimates $\bar{K}_{ij\cdot}$, we used the delta-method approximation to the variance of a ratio described in Baddeley et al. (2015). We thus calculated a standard error and made approximated 95% confidence intervals (grey shadings in Fig. 6) for the K-function. K-functions of the bubble experiment array indicate small-scale regularity with an inhibitory effect up to 0.5 mm on average in most of the cells, except in cells 5 ppm, 8 L min^{-1} and 5 ppm, 10 L min^{-1}, where the inhibitory effect is almost 1.0 mm. For larger distances, there is a tendency to clustering in most patterns, except perhaps, in those of the first cell 5 L min^{-1}, 5 ppm where it is seen that the K-functions oscillate around CSR line (horizontal zero). Furthermore, one would suspect that the 5 L min^{-1}, 5 ppm case behaves differently than the others

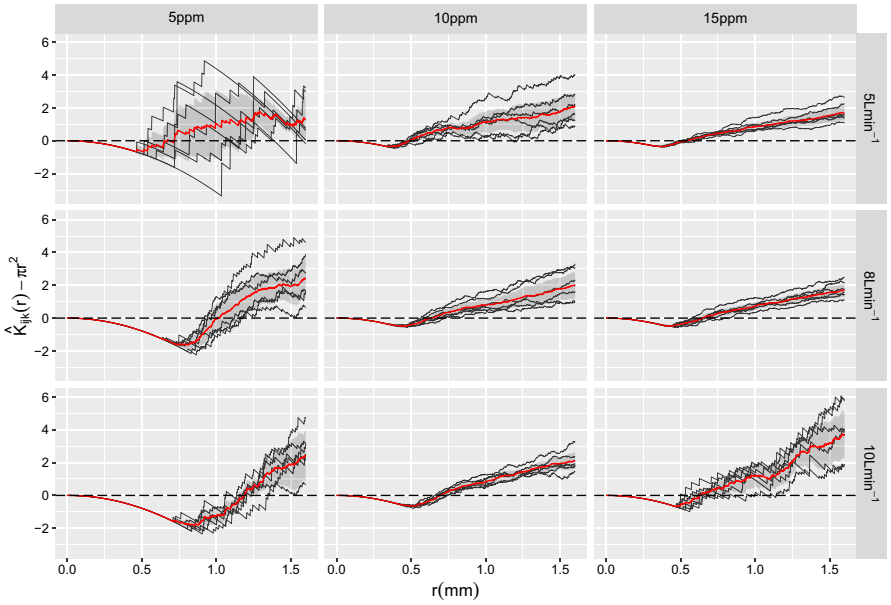

Fig. 6 General arrangement of estimates of centred K-functions (black lines) and pooled K-functions (red lines) of point patterns for floating bubbles with three frother concentration levels (columns) and three volumetric airflow levels (rows). The grey shading in each panel corresponds to pointwise 95% confidence interval based on the observed within cell sample variance in the estimated K-function (color figure online)

as it runs close to a Poisson point pattern, while the spatial patterns of the other cases seem to be similar independently of the volumetric airflow rate level.

The tests were carried out using the integration interval $T = (0, r_0]$, whose upper limit is recommended to be taken as (see Hahn and Vedel Jensen 2016 and references therein) $r_0 = 1.25/\sqrt{\max \hat{\lambda}_{ij}}$, obtaining an upper integration bound $r_0 = 1.57$ mm. We implemented the tests with 500,000 random permutations. For the interaction effect, we have a significant p-value associated with the residuals given in Eq. (21), $\hat{p}_{\hat{R}_{ijk}} = 0.0275$, analogously $\hat{p}_{\hat{R}^{\dagger}_{ijk}} = 0.0153$ in the case of the residuals given in Eq. (22). For the main effects, we have p-values of zero in the case of the frother concentration factor for both residuals as well as p-values of zero in the additive effect. Finally, for the volumetric airflow rate factor, we have also significant p-values ($\hat{p}_{\hat{R}_{ijk}} = 0.0110$ and $\hat{p}_{\hat{R}^{\dagger A}_{ijk}} = 0.0059$).

According to the tests, the flotation point patterns have different statistical behaviour in terms of their interaction structure, and this difference is explained by the levels of the row and column factors. We conclude that as the concentration and volumetric airflow rate levels grow simultaneously, the aggregation of the bubbles stabilises itself (except in the most extreme combination 15 ppm and 10 L min^{-1}). The variance of the K-functions seems to stabilise as well, having its minimum at the combination 15 ppm and 8 L min^{-1}; interestingly, by this combination, the bubble point patterns look nearest to the CSR. Therefore, if the need is to have CSR point patterns (to

eventually apply stochastic geometry in subsequent analyses), the best combination of levels would be 15 ppm and 8 L min^{-1}.

5 Discussion

We have implemented a method for the analysis of experiments with two fixed factors in the presence of replicates through approximate permutation tests when the observations are functional second-order descriptors. To achieve this aim, we have been motivated by the work of several authors. For example, while we follow (Zhang 2013) using Fisher-based statistics, our method engages weighted means instead of classical ones. Our strategy for approaching empirical p-values is focused on the permutation of residuals recommended by Anderson and Braak (2003) as a substitute for reconstructed observations (Wilson 1998; Ramón et al. 2016), and the weightings for the residuals are inspired by the estimation of intensity suggested in Hahn 2012 and Baddeley et al. (2015).

We have focused on the case of balanced experiments with two factors and the same number of replicates within cells as our data set motivated such assumption. The statistical tests have been demonstrated by simulation (the validity and power). Our tests require exchangeable units (residual functions), and this assumption can be approximately achieved through the independence of point patterns in the sample. We have seen that full-model residuals have shown satisfactory performance in all cases; therefore, they are applicable for testing main effects and interaction. As an alternative that encompasses all cases, they are the ones we would recommend for a general analysis of variance. However, when we have the specific objective of testing interaction, the saturated-model residuals are the best in both performance and power. For the particular case of the main effects, we have observed that both the full-model residuals and the reduced-model residuals have similar performance, the latter having overall better power.

Our approach can be enhanced in many ways depending on the questions related to the experiment itself. A possible straightforward generalisation consists of considering unbalanced experiments, or more ambitiously, non-orthogonal designs. Our test statistics are defined through integral distances between the estimates of K-functions, their means and variances, implying that the power of the tests depends on the interval of integration $T = (0, r_0]$ (Choi and Hall 1999; Hahn 2012). So, further functional distances that are not as sensitive to the r_0 parameter could be used instead. One could think of a non-condensed version, i.e. with no integration over T of the Fisher-based statistics, to better consider applying the global rank envelope test in the sense of Mrkvička et al. (2020b).

Although we have focused mainly on Ripley's K-function, these methods could be used with other descriptors such as the L- function (Besag 1977), the pair-correlation function $g(r)$, the nearest-neighbour distance distribution $F(r)$, the empty space function $G(r)$, or the J-function (van Lieshout and Baddeley 1996; Illian et al. 2008). Some of these functional descriptors could be problematic, for instance, the estimator of the pair-correlation function tends to be unreliable at small distances and the estimator of the J-function at long distances, so the integration bounds must be modified to include

only valid regions. The weighted means may not be applicable in all those cases, but the classical ones might replace them.

Regarding the flotation experiment, we applied a scaled Poisson model to the bubble counts in the responses. We observed significant differences amongst the levels of the factors as well as an extra-Poisson variation within the groups; this suggests that a spatial interaction structure may be achieved by properly combining the treatments. Through the K-function, we have discovered that the patterns exhibit a small-scale regularity and large-scale clustering. This aspect represents an advance in the assumptions usually made in the literature of flotation experiments since CSR patterns have been assumed (see e.g. Emery et al. 2012; Kracht et al. 2013). We have used an analysis of variance approach to explaining how the structural variation (aggregation) of the bubble point patterns is significantly affected by the factors separately and, most importantly, by their interaction. Although there are two combinations of levels (5 ppm and $5\,\mathrm{L\,min^{-1}}$, as well as 15 ppm and $10\,\mathrm{L\,min^{-1}}$) that seem different at first glance in Fig. 3, they also present K-functions that clearly differ from their counterparts. We have verified that these differences are not only a visual assessment but also statistically significant through our procedure.

An important covariate associated with bubbles is their diameter. The diameter can be attached, as a mark, to the centre location of the bubble. In this case, it is natural to represent a marked point process as a collection of pairs $\{(\mathbf{u}_i, m_i)\}_{i=1}^{p} \subset W \times M$, where M is the *space of marks* (Penttinen et al. 1992; Møller and Waagepetersen 2004; Illian et al. 2008). An attractive extension of the present work would relate the marks with an unobserved spatially continuous field that might influence the locations, i.e. preferential sampling. In practice, this would impose a geostatistical model for bubble size on each point pattern as long as the dependence can be statistically proven (see, e.g. Mrkvička et al. 2020a).

Acknowledgements We are indebted to Dr Aila Särkkä and Dr Edith Gabriel for their careful comments on an earlier draft. We would like to thank Project CORFO, SMI-ICE-CHILE 13CE12-21844-F1-L1-P3, "Frother Roles Characterization in a Laboratory Mechanical Flotation Cell", for their kindness in providing the data set analysed. Jonatan A. González and Jorge Mateu are partially funded by Grant MTM2016-78917-R from the Spanish Ministry of Science and Education. Bernardo Lagos-Álvarez thanks VRID Grant 216.014.026-1.0, from University of Concepción.

References

Abramovich F, Angelini C (2006) Testing in mixed-effects FANOVA models. J Stat Plan Inference 136(12):4326–4348

Anderson M, Braak CT (2003) Permutation tests for multi-factorial analysis of variance. J Stat Comput Simul 73(2):85–113

Baddeley A, Boyde A, Reid S, Howard C (1987) Three-dimensional analysis of the spatial distribution of particles using the tandem-scanning reflected light microscope. Acta Stereol 6(supplement II):87–100

Baddeley A, Moyeed R, Howard C, Boyde A (1993) Analysis of a three-dimensional point pattern with replication. J Roy Stat Soc Ser C (Appl Stat) 42(4):641–668

Baddeley A, Møller J, Waagepetersen R (2000) Non- and semi-parametric estimation of interaction in inhomogeneous point patterns. Stat Neerl 54:329–350

Baddeley A, Rubak E, Turner R (2015) Spatial point patterns: methodology and applications with R. Chapman & Hall Interdisciplinary Statistics Series. CRC Press, Boca Raton

Bagchi R, Illian JB (2015) A method for analysing replicated point patterns in ecology. Methods Ecol Evol 6(4):482–490
Besag J (1977) Contribution to the discussion of Dr Ripley's paper. J R Stat Soc Ser B (Stat Methodol) 39:193–195
Chen F, Gomez C, Finch J (2001) Technical note bubble size measurement in flotation machines. Miner Eng 14(4):427–432
Chiu SN, Stoyan D, Kendall WS, Mecke J (2013) Stochastic geometry and its applications. Wiley series in probability and statistics, 3rd edn. Wiley, Chichester
Choi E, Hall P (1999) Nonparametric approach to analysis of space-time data on earthquake occurrences. J Comput Graph Stat 8:733–748
Cressie NAC (1993) Statistics for spatial data, revised. Wiley, New York
Cuevas A, Febrero M, Fraiman R (2004) An ANOVA test for functional data. Comput Stat Data Anal 47(1):111–122
Daley D, Vere-Jones D (2003) An introduction to the theory of point processes: volume I: elementary theory and methods, 2nd edn. Springer, New York
Diggle PJ (2013) Statistical analysis of spatial and spatio-temporal point patterns. Chapman & Hall monographs on statistics & applied probability, 3rd edn. CRC Press, Boca Raton
Diggle PJ, Lange N, Beneš FM (1991) Analysis of variance for replicated spatial point patterns in clinical neuroanatomy. J Am Stat Assoc 86(415):618–625
Diggle PJ, Mateu J, Clough H (2000) A comparison between parametric and non-parametric approaches to the analysis of replicated spatial point patterns. Adv Appl Prob 32(2):331–343
Efron B (1979) Bootstrap methods: another look at the jackknife. Ann Stat 7(1):1–26
Emery X, Kracht W, Egaña Á, Garrido F (2012) Using two-point set statistics to estimate the diameter distribution in Boolean models with circular grains. Math Geosci 44(7):805–822
Ferraty F, Vieu P, Viguier-Pla S (2007) Factor-based comparison of groups of curves. Comput Stat Data Anal 51(10):4903–4910
Gomez C, Finch J (2007) Gas dispersion measurements in flotation cells. Int J Miner Process 84(1):51–58
Gómez C, Mesías J, Álvarez J (2016) Bubble surface area flux and performance in laboratory flotation testing. In: XXVIII international mineral processing congress proceedings. Canadian Institute of Mining, Metallurgy and Petroleum
Górecki T, Smaga Ł (2015) A comparison of tests for the one-way ANOVA problem for functional data. Comput Stat 30(4):987–1010
Hahn U (2012) A studentized permutation test for the comparison of spatial point patterns. J Am Stat Assoc 107(498):754–764
Hahn U, Vedel Jensen EB (2016) Hidden second-order stationary spatial point processes. Scand J Stat 43(2):455–475
Ho LP, Chiu SN (2006) Testing the complete spatial randomness by Diggle's test without an arbitrary upper limit. J Stat Comput Simul 76(7):585–591
Illian J, Penttinen P, Stoyan H, Stoyan D (2008) Statistical analysis and modelling of spatial point patterns. Statistics in practice. Wiley, London
Kracht W, Emery X, Paredes C (2013) A stochastic approach for measuring bubble size distribution via image analysis. Int J Miner Process 121:6–11
Landau S, Everall IP (2008) Nonparametric bootstrap for K-functions arising from mixed-effects models with applications in neuropathology. Stat Sin 18(4):1375–1393
Laskowski J (2001) Coal flotation and fine coal utilization. Developments in mineral processing. Elsevier Science, Amsterdam
McCullagh P, Nelder JA (1989) Generalized linear models. Chapman & Hall monographs on statistics and applied probability, 2nd edn. CRC Press, Boca Raton
Miskovic S, Luttrell G (2012) Comparison of two bubble sizing methods for performance evaluation of mechanical flotation cells. In: Young CA, Luttrell GH (eds) Separation technologies for minerals, coal, and earth resources. Society for Mining, Metallurgy, and Exploration, Englewood
Møller J, Waagepetersen RP (2004) Statistical inference and simulation for spatial point processes. Chapman & Hall monographs on statistics & applied probability. CRC Press, Boca Raton
Mrkvička T, Dvořák J, González JA, Mateu J (2020a) Revisiting the random shift approach for testing in spatial statistics. Spat Stat. https://doi.org/10.1016/j.spasta.2020.100430
Mrkvička T, Myllymäki M, Jílek M, Hahn U (2020b) A one-way ANOVA test for functional data with graphical interpretation. Kybernetika 56(3):432–458

Myllymäki M, Särkkä A, Vehtari A (2014) Hierarchical second-order analysis of replicated spatial point patterns with non-spatial covariates. Spat Stat 8:104–121
Penttinen A, Stoyan D, Henttonen HM (1992) Marked point processes in forest statistics. For Sci 38(4):806–824
Ramón P, de la Cruz M, Chacón-Labella J, Escudero A (2016) A new non-parametric method for analyzing replicated point patterns in ecology. Ecography 39(11):1109–1117
Ramsay JO, Silverman BW (2005) Functional data analysis, 2nd edn. Springer, New York
Ripley BD (1977) Modelling spatial patterns (with discussion). J R Stat Soc Ser B (Stat Methodol) 39(2):172–212
Ripley BD (1988) Statistical inference for spatial processes. Cambridge University Press, Cambridge
Schlesinger ME, King MJ, Sole KC, Davenport WG (2011) Extractive metallurgy of copper, 5th edn. Elsevier Science, Amsterdam
van Lieshout MNM, Baddeley AJ (1996) A nonparametric measure of spatial interaction in point patterns. Stat Neerl 50(3):344–361
Wilson HE (1998) Statistical analysis of replicated spatial point patterns. PhD thesis. Lancaster University
Zhang JT (2013) Analysis of variance for functional data. Chapman & Hall monographs on statistics & applied probability. CRC Press, Boca Raton